Author(s): Molaiyan, Palanivel; Välikangas, Juho; Sliz, Rafal; Ramteke, D. D.; Hu, Tao; Paolella, Andrea; Fabritius, Tapio; Lassi, Ulla

Title: Screen-Printed Composite LiFePO4-LLZO Cathodes Towards Solid-State Li-ion Batteries

Year: 2024

Version: Published version

ChemElectroChem

Research Article
doi.org/10.1002/celc.202400051

Chemistry Europe
European Chemical Societies Publishing

www.chemelectrochem.org

Screen-Printed Composite $LiFePO_4$-LLZO Cathodes Towards Solid-State Li-ion Batteries

Palanivel Molaiyan,*[a] Juho Valikangas,[a] Rafal Sliz,[b] D. D. Ramteke,[c] Tao Hu,[a] Andrea Paolella,[d] Tapio Fabritius,[b] and Ulla Lassi*[a, e]

$LiFePO_4$ (LFP) is widely used as cathode material for its low cost, high safety, and good thermal properties. It is one of the most exploited cathode materials for commercial Li-ion batteries (LIBs). Herein, we present a screen-printing method to prepare a LFP composite cathode, and a rational combination of the typical composite solid electrolytes (CSE) consisting of polyethylene oxide (PEO)/Li-salt (LiTFSi) electrolyte with ceramic filler (LLZO or $Li_{6.4}La_3Zr_{1.4}Ta_{0.6}O_{12}$ (LLZTO)) has been successfully demonstrated for SSB. The prepared CSE offers: i) a promising ionic conductivity (0.425 mS cm^{-1} at 60 °C), ii) a wide electrochemical window (>4.6 V), iii) a high Li-ion transference number ($tLi_+ = 0.44$), iv) a good interfacial compatibility with the electrode, v) a good thermal stability, and vi) a high chemical stability toward Li metal anode. The Li/CSE/Li symmetric cells can be cycled for more than 1000 h without Li-dendrites growth at a current density of 0.2 mA cm^{-2}. The final cell screen-printed LFP composite cathode (LFP + LLZO)//Li metal displays a high reversible specific capacity of 140 mAh g^{-1} (0.1 C) and 50 mAh g^{-1} (0.5 C) after 1st and 500th cycles.

Introduction

EVs and grid storage are needed to reduce CO_2 emissions thus limiting the effects of climate change.[1] LIBs are currently the most promising technology for energy storage devices but suffer from safety issues due to the use of organic liquid electrolytes (LE).[2] A possible solution to overcome the safety concerns can be obtained by switching from liquid-state to solid-state electrolytes (i.e., the transition towards Solid-state batteries (SSBs).[3] SSBs have captured battery manufacturers' attention with the promise of improving the safety, cost, energy density, and range of EVs.[4] However, a solid electrolyte (SE) material having high stability, high processability, and ionic conductivity is not identified yet.[5,6]

Despite the efforts to improve the materials 'properties, insignificant attention has been paid to a suitable production process and cost-saving techniques (Table 1).[2,7,8] Manufacturing techniques based on printing methods (Screen printing, 3D printing, etc.) are promising approaches to fabricated battery components and whole batteries for SSBs and LIBs.[9,10] Usually, screen printing technologies have been utilized for the fabrication of scalable batteries with different shapes:[11,12] several studies are dedicated to 3D layer-by-layer structures, which can provide a pathway to the manufacture of LIBs and a variety of shapes.[7,13] Printable battery materials in their high speed to build ultra-thin printed batteries that are flexible, safer, and more environmentally friendly. In this regard, many efforts have been dedicated to developing new materials and low-cost manufacturing technologies to reduce the cost and fast production and customize designs for LIBs.[14,15]

Table 1. A comparison between blade coating and screen-printing methods.

	Blade Coating	Screen printing
Benefits	Well known process	Little/No waste of materials, Custom design shape & Lower drying costs
	Large area and good uniformity	Good uniformity and large area printing, Layer by layer printing
	Little/No waste of materials	Less assembly steps and a large range of thickness Suitable for LIB/SSB productions
Challenges	No flexible shape or design	New manufacturing techniques in battery productions
	Higher cost for drying, Low solid content & Internal resistance	Low viscosity for ink or paste is not suitable

[a] P. Molaiyan, J. Valikangas, T. Hu, U. Lassi
Research Unit of Sustainable Chemistry, University of Oulu, FI-90570, Oulu, Finland
E-mail: palaniiiphys87@gmail.com
ulla.lassi@oulu.fi

[b] R. Sliz, T. Fabritius
Optoelectronics and Measurement Techniques Unit, University of Oulu, 90570 Oulu, Finland

[c] D. D. Ramteke
Fibre and Particle Engineering Research Unit, University of Oulu, FI-90570, Oulu, Finland

[d] A. Paolella
Dipartimento di Scienze Chimiche e Geologiche, Università degli Studi di Modena e Reggio Emilia, Via Campi 103, 41125 Modena, Italy

[e] U. Lassi
Kokkola University Consortium Chydenius, University of Jyvaskyla, FI-67100, Kokkola, Finland

Supporting information for this article is available on the WWW under https://doi.org/10.1002/celc.202400051

$LiFePO_4$ (LFP) is a promising cathode material. Despite warnings that could reduce global EV sales in 2030, LFP-based LIBs remain in high demand. SSBs that can harness a lithium metal operation could give higher energy density or keep them on par despite using the lower voltage but earth-abundant LFP.[16,17] It currently overcomes supply chain issues and high prices, as high-cost raw materials such as cobalt and nickel are not required for the cathode.[17] They offer higher energy density than conventional LIBs, significantly shorter charging time due to superior charge and discharge performance, and lower costs of using less expensive materials. LFP-based batteries are emerging as one of the top contenders in space, with 17% of the world's EV market share.[2,18]

The polymer-based SEs exhibit sufficiently high ionic conductivity and excellent thermal stability, high environmental stability, excellent flexibility, and scalable processing with low cost.[19] Polyethylene oxide (PEO)-based. However, they have some drawbacks: low ionic conductivity at room temperature and oxidative decomposition potential (below 4 V).[20,21,22] Out of various polymers, PEO-based electrolytes are the most widely studied for SSBs with their advantage of good electrochemical stability with Li anode, processibility, and compatibility. Ceramic-based solid-state electrolytes (SEs) may offer improved conductivity and electrochemical windows.[23] Presently, the most common classes of SEs are polymers and ceramics such as oxides (e.g LLZO), phosphate (e.gNASICON), sulfides (e.g.$Li_{10}GeP_2S_{12}$, Li_6PS_5X), and halides (e.g Li_3InCl_6, Li_3YBr_6).[2,18] In the development of composite solid electrolytes (CSEs) or hybrid electrolytes incorporation of a small amount (up to 40 wt%) of inorganic active fillers (perovskite, garnet, LISICON, etc.) in the polymer matrix has already been widely reported.[22,23] Inorganic active fillers could form continuous ion channels in the bulk region of CSEs and facilitate fast-ion transport to provide higher ionic conductivity without compromising the flexibility of the matrix.[24] Still, there is plenty of room to develop better CSEs to achieve higher ionic conductivity without detracting its mechanical properties.[25]

Here we report a new screen-printing method to prepare SSB cathodes based on LFP (LFP + LLZO) with two different CSEs, which one is based on LLZO (CSE1) and the second LLZTO (CSE2) which are blended in PEO/LiTFSi. As a result, Li//SCEs// printed LFP cells deliver initial charge/discharge capacities of 142 mAh g^{-1} with a rate of 0.1 C and 35 mAh g^{-1} at 500 cycles with a rate of 0.5 C. Using CSEs, we demonstrate the stable operation of SSBs with a screen-printed LFP cathode. This work provides a novel strategy for designing screen-printed cathode composite, understanding the mechanism, and printing approach, and challenging the low ionic conductivity in CSE for SSB applications.

Results and Discussion

Screen printing is a mature technology that can easily be scaled up for developing appropriate catholytes for SSBs.[9,26] A screen printing approach for cathode composite (LFP + LLZO) is demonstrated for SSB applications (Figure 1a). The ink formulation contains a composite cathode slurry composed of 80 wt% of LFP powder with 5 wt% of LLZO (denoted as SP1) in DMF solvent. The formulated ink is printed on Al foil as shown in Figure 1b. SEM images of the cathode composite SP1, which is systematically aligned in uniform printing (Figure 1c–d). The cross-section image shows that the solid electrolyte particles are well interconnected with the cathode as a result of good contact during the printing stage. Figure 1e illustrates the surface morphology of the screen-printed cathodes. A subtle pattern, akin to the mesh pattern used in screen printing, is discernible. Moreover, the measured surface roughness values (Sq = 9.26 μm and Sa = 7.36 μm) quantitatively affirm the printed cathodes' adequate smoothness. The EDX analysis (Figure S1) shows the amount of chemical composition of the cathode composite. The SEM images of the LFP composite cathode mix with Li salt, which is very well connected to the cathode particle.[27] In addition, SEM images of CSE1 and CSE2 are presented in Figure S2 & S3.

As seen by the thermogravimetric (TG) (Figure 2a), pure PEO exhibits thermal stability up to 300 °C. Beyond 300 °C, however, the sample experiences a sudden and rapid mass loss. The weight loss observed in CSE1 and CSE2 is related to decomposition reactions. PEO is known to decompose thermally at high temperatures: for the CSE1 sample, it is possible to observe a weight loss until 454 °C, resulting in the production of volatile compounds (e.g ethylene glycol) and consequently in a decrease in the material's mass. Similarly, in CSE2, weight loss begins at 343 °C and concludes at 446 °C, indicating a similar PEO breakdown mechanism. Within their respective temperature ranges, CSE1 and CSE2 membranes both display a level of thermal resistance that makes them ideal for use as electrolytes.[28–30]

Figure 2b–c shows the temperature dependence of the total ionic conductivity of CSE1 and CSE2 evaluated via electrochemical impedance spectroscopy (EIS) from 30 to 90 °C by using stainless steel disks as blocking electrodes in symmetric cells. The temperature depends on measurements of the Nyquist plots representing that the depressed semicircle (bulk impedance) is accompanied by a straight line at a low frequency which expresses the polarization of electrolyte-electrode at the blocking electrodes. The semicircle disappears as temperature increases due to the reduction of the total resistance resistance.[31,32] By incorporating LLZO (CSE1) and LLZTO (CSE2) particles as fillers into the PEO-based electrolytes the bulk conductivity was found to be 5.85×10^{-6}, 7.40×10^{-5} S cm^{-1} at RT, and the ionic conductivity of 1.06 and 1.45 S cm^{-1} at 90 °C, respectively (Figure S4). Similarly, Zheng Zhang et al reported that the composite solid electrolytes (CSEs) used two different oxide fillers 10 wt% of LLZO and LLZTO ceramic filler offered the ionic conductivity of 1.7×10^{-4} S cm^{-1} at 30 °C.[33] The cationic lithium transference number was investigated by Sorensen and Jacobsen method.[34–36] t_{Li+} value was 0.41 and 0.44 for CSE1 and CSE2, indicate almost no difference (Figure S4). The electrochemical stability of CSE is verified by LSV shown in Figure 2d. LLZO (CSE1) and LLZTO (CSE2) present electrochemical stability to 5 and 5.2 V vs. Li/Li^+.

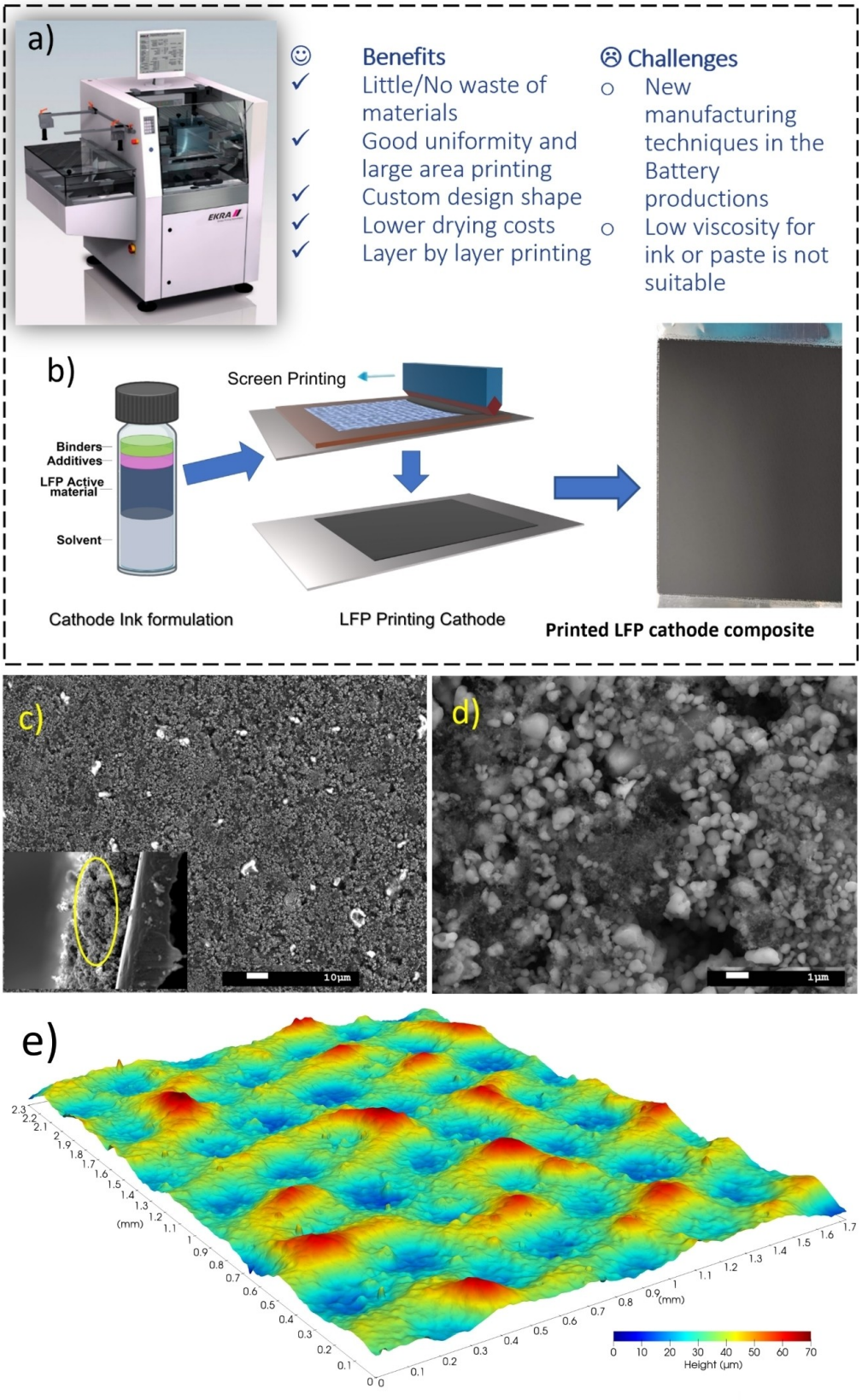

Figure 1. a) A photograph of lab scale screen printing device b) Ink formation and the screen-printed process followed by LFP printed layers are demonstrated. The ink contains LFP cathode materials, LLZO, PVDF, carbon black, and DMF as a solvent. A photograph of Screen printed LFP composite cathode. c-d) SEM images of Screen-printed composite cathodes SP1 (LFP + LLZO) with different magnifications. e) Surface morphology of the screen-printed cathodes.

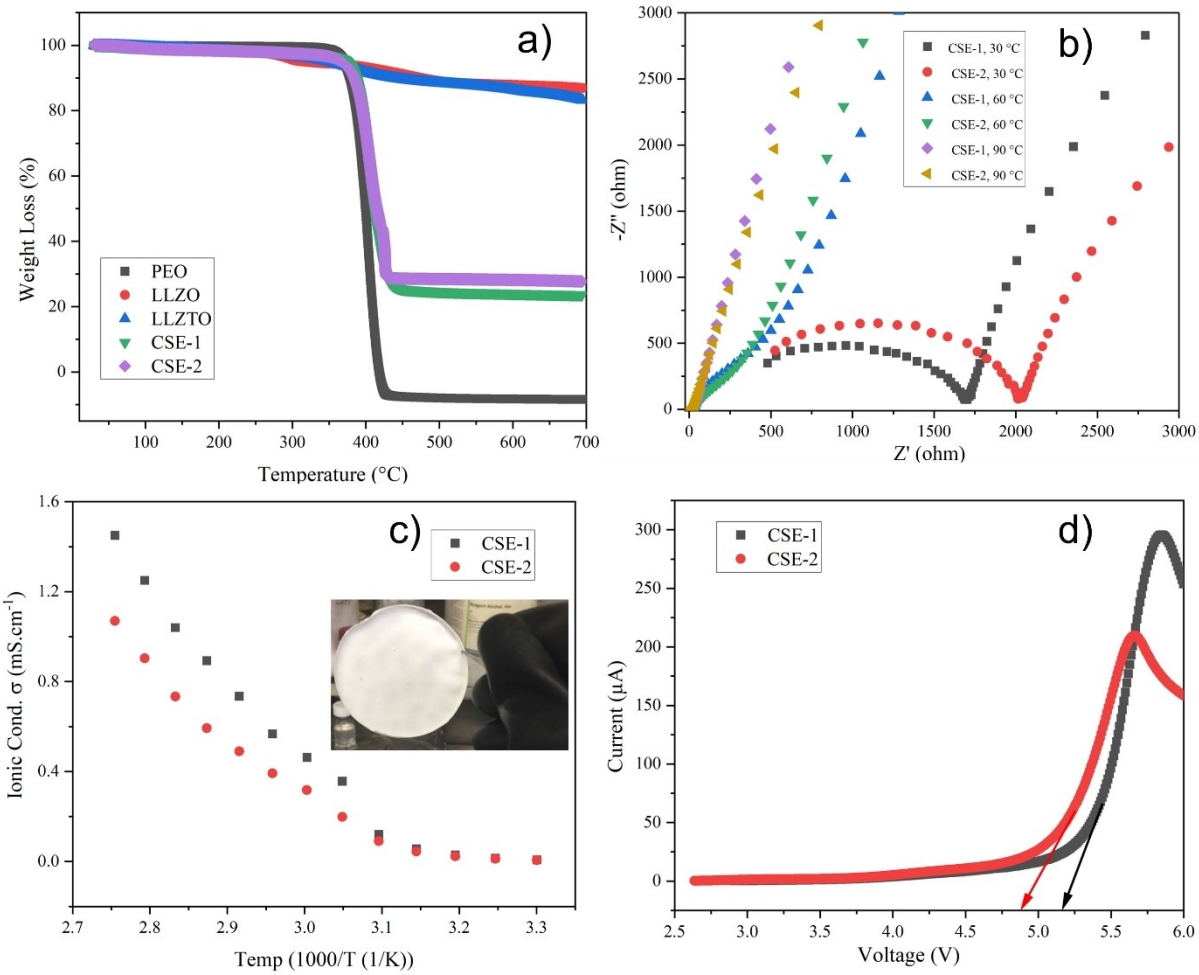

Figure 2. a) TGA measurements of PEO, LLZO, LLZTO, CSE1, and CSE2. b) The Nyquist plots of the two membranes for CSE1 and CSE2. c) Temperature-dependent ionic conductivity of CSE1 and CSE2. d) LSV measurement of the two membranes.

Figure 3a and **3 c** show the charge/discharge results of the two membranes of CSE1 and CSE2 in symmetrical Li///Li cell configurations. The stripping and plating process was performed at a current density of 0.1mAh/cm^2 (0.5 h of charge and discharge) at a temperature of 60 °C. The time-dependent voltage profile of the CSE1 and CSE2 with Li vs. Li half-cell exhibits the deposition and dissolution curves of lithium with no detrimental polarization effects. CSE1 and CSE2 exhibit a polarization voltage of ±38 mV, whereas CSE1 shows a reduction in the polarization voltage until 400 h and again starts to increase and stabilize from 700 h but with CSE2 electrolyte voltage was stable for 1000 h. As the voltage was stable for 1000 h it implies that neither dendrites were formed nor unstable SEI is formed on Lithium metal in contact with the electrolytes. Figure 3b and **3 d** show the Nyquist plot of impedance spectroscopy during galvanostatic cycling of CSE1 and CSE2. The interfacial resistance of the CSE1 electrolyte seems to increase during cycling whereas the interfacial resistance in CSE2 is not much higher than CSE1, which can imply in the voltage vs. time profile of the galvanostatic cycling.

In Figure 4a the electrochemical performance of the screen-printed composite cathode SP tested with two different membranes (CSE1 and CSE2) is compared in coin cell configuration. The voltage profiles clearly show a plateau at 3.45 V for both cells, which is typically related to the lithiation/delithation process of LFP cathodes. The initial capacity of both membranes with SP1 delivers a specific capacity of around 140 mAh g^{-1} (0.1 C). Figure 4b shows the rate capabilities of Li/CSE1//SP1 and Li/CSE2//SP1 at different current densities: with a comparable initial capacity of around 140 mAh g^{-1} at 0.1 C. Generally, CSE1 shows better capacity retention at all C-rates when compared to CSE2 with the same initial capacity of 135 mAh g^{-1} but capacity fades sharply after a few cycles in CSE2 and CSE1 due to the lower ionic conductivity of CSE. The Coulombic efficiency (CE) is stable in both membranes with LFP + LLZO cathodes. Figure 4d shows the Nyquist plot of the full cells before and after cycling forming SEI that is after the third cycle to check the interfacial resistance between two CSEs with SP1. The interfacial resistance is lower in the CSE1 when compared with the CSE2 (Figure S5). This was repeated with the SP2 composite cathodes which is correlated with Figure S6. After Ragone tests the cells are kept for long cycling at 0.5 C for 500 cycles. Both cells start to decay after a few cycles and reach 50 mAh g^{-1} and 30 mAh g^{-1} at 500th cycles with CSE2 and CSE1

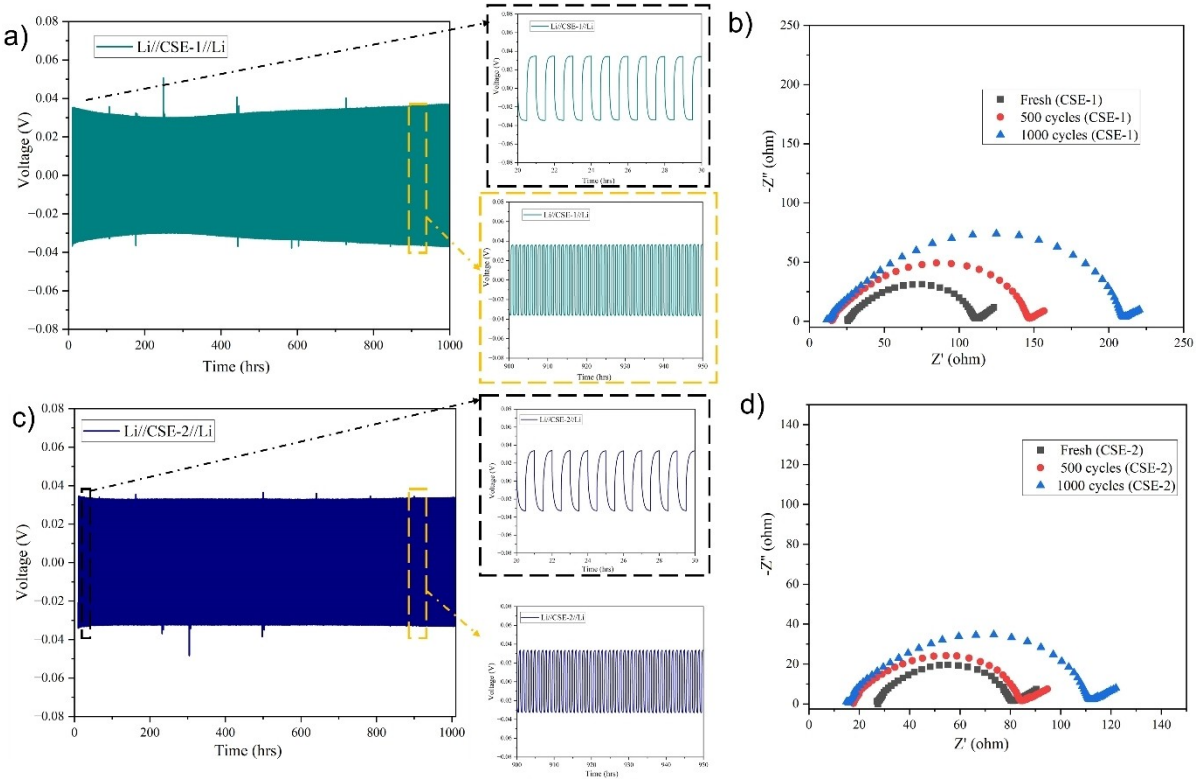

Figure 3. The symmetric cells of Li//CSE1//Li (a) and Li//CSE2//Li (c) at 0.1 mAh/cm^2. b & d) The EIS studies of the CSE1 and CSE 2 membranes for the fresh, 500, and 1000 cycles.

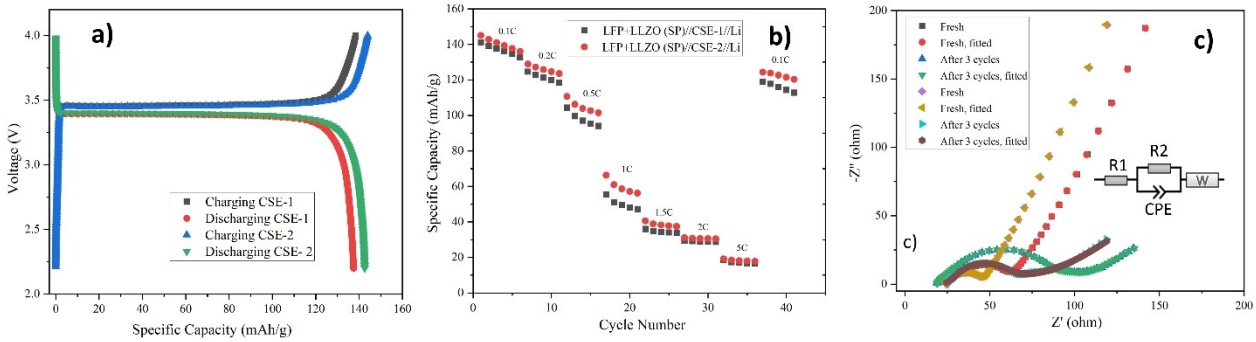

Figure 4. a) The electrochemical performances of Screen printed LFP cathodes SP1 with CSE1 and CSE2. a) Voltage profiles of first charging and discharging cycles. b) rate capability test. c)impedance measurements of fresh cells, and 3rd cycles.

with stable CE (Figure 4c). On the contrary, the composite cathode containing Li salt (SP2 with CSE1) shows a higher initial capacity but there is sharp decay in the capacity and reaches 35 mAh g^{-1} at the 500th cycle with fluctuations in columbic efficiency, and with CSE2 the capacity was reduced for a few cycles and reach stability and reach 20 mAh g^{-1} with stable CE (Figure S6). The Nyquist plot shows that the interfacial resistance is low with CSE2 when compared with CSE1 with SP1.

Conclusions

In summary, we present the preparation of a screen-printed composite (LFP-LLZO) as the cathode in combination with two different CSEs for SSBs prudently designed and systematical studied. As a result, the combined CSE offers promising ionic conductivity (0.425 mS cm^{-1} at 60 °C), a wide electrochemical window (> 4.6 V), a high Li-ion transference number ($tLi_+ =$ 0.44), and good interfacial compatibility with the electrode, good thermal stability, and good interaction with Li metal stability. The Li/CSE/Li symmetric cells can be stable for more than 1000 hrs without Li-dendrites formation at a current density of 0.2 mA cm^{-2}. The screen-printed LFP-based full cell with composite cathode (LFP + LLZO), and Li metal displays a high reversible specific capacity of 140 mAh g^{-1} (0.1 C) and 50 mAh g^{-1} (0.5 C) after 1st and 500th cycles. The development of printable LFP cathodes designed for SSBs represents a valuable step toward an industrial scale and customizable energy

storage devices. The optimization and design of LFP cathode and composite SEs are still underway, of which ink formulation, ion conductivity, and stability are essential. Summarizing all these results, the developed printable LFP is a promising candidate for further development of various SSB applications.

Experimental Methods

Materials: PEO powder (MW = 6*10^5 g/mol) was dried under a high vacuum for 48 h at 50 °C. The anhydrous acetonitrile (ACN, 99.9%), polyvinylidene fluoride (PVdF), carbon black, and 1-methyl-2-pyrrolidinone (NMP) were purchased from Sigma-Aldrich. LiTFSi (99.9%) was obtained from Kishida. The materials for LLZO and LLZTO were purchased from Ganzhou LuckPr Advanced Materials Co., Ltd, China.

Membrane preparations: The composite polymeric electrolytes (CSEs) were prepared by conventional solution casting. PEO and LiTFSI at a molar ratio of 20:1 were dissolved in 8 mL of ACN and stirred overnight until a homogenous solution was obtained, simultaneously 30 wt% of ceramic material (LLZO (CSE1), LLZTO (CSE2)) was added to 12 mL of ACN and stirred for more than 24 hours until a uniform solution was obtained and both solutions were mixed and stirred for overnight until a homogenous solution was obtained. The solution was cast on a Teflon tray and left to evaporate the ACN slowly for 24 hours at room temperature. The SPE was formed was dried at 50 °C for 24 h under vacuum. The entire synthesis was carried out in a glovebox under an argon atmosphere (O_2 and H_2O < 0.1 ppm). The CSE is called LLZO (CSE1) and LLZTO (CSE2).

Screen Printing Approach for LFP cathodes: An LFP-based cathode composite slurry was prepared with a ThinkyMixer ARE-250 (Thinky Corporation, Tokyo, Japan). The slurry composition (ink formulation) was 5 wt% polyvinylidene fluoride (PVdF, Kureha #1100), 10 wt% Super P (Timcal C45), 80 wt% LFP active material, and 5 wt % LLZO, with DMF (DMF, Alfa Aesar, anhydrous 99.5%) as a solvent. The slurry was screen printed and deposited on aluminum foil using 20 μm applicators. The printing process was carried out with an Ekra E2 screen printer and a Koenen stencil (W-Øx22.5°, VA 165–0.05 mm)[26] at a speed of 40 mm/s. Following the printing, the cathode layers were dried on a hot plate at 80 °C for 1 hour.

Morphology studies: The cross-section of cathodes and composite solid electrolytes were analyzed using a JEOL JSM-7900F Schottky Field Emission Scanning Electron Microscope (FESEM). The device is equipped with an energy-dispersive X-ray spectrometer (EDS) and AZtec software of Oxford Instruments. The analysis was done at 15 kV and a working distance of around 10 mm. The surface morphology analysis was performed using a Bruker ConturGT profilometer in Vertical Scanning Interferometry (VSI) mode. The Gwyddion and Paraview software were utilized to map the acquired profilometry data and to extract the numerical values of surface roughness.

Thermal analysis: The milled samples were subjected to thermogravimetric analysis (TGA) with an SDT650 analyzer from TA Instruments (USA). The samples were heated at a rate of 10 °C/min from 30 to 700 °C in a nitrogen environment. The collected data was then examined with TRIOS and OriginPro software.

Electrochemical measurements: Ionic conductivity and transference number were taken using Eq. 1 and 2. A Symmetric 2032 coin-cell setup with blocking and non-blocking electrodes was assembled in a glove box filled with ultra-high purified argon (O_2 and H_2O < 0.1 ppm. The diameter of both the electrodes and electrolyte membranes was 12 and 16 mm, respectively. The conductivity of the electrolyte was determined by electrochemical impedance spectroscopy using the Palmsens instrument. Tests were carried out at a 30 to 90 °C temperature range with 10 mV amplitude at a frequency range of 1 MHz to 1 mHz. The bulk conductivity of the electrolyte was calculated based on resistance extracted from the intercept of the high-frequency branch of the Nyquist plot with the x-axis:

$$\sigma = l/R_b A, \tag{1}$$

where ***l*** is the thickness of the electrolyte film (in cm), R_b is the bulk resistance (in Ω), and A is the contact area of the electrolyte (in cm^2). Activation energies were calculated assuming Arrhenius-type behavior. Li//CSE//Li cells were kept for 2 h at each temperature before the measurements. The Li^+ transference number of CPEs was assembled in a coin cell format (Li||CPE||Li). The cationic lithium transference number is one of the parameters for characterizing the CSEs, which explains the contribution of the positive charge to the total conductivity. It was investigated by sorensen and Jacobsen and calculated according to Eq. 2[36,37]

$$t_+ = \frac{1}{1 + Z_d/R_b} \tag{2}$$

Where Z_d is the impedance at low frequency (< 0.01 Hz) due to Warburg diffusion. The electrochemical stability window of the membranes was studied by linear sweep voltammetry (LSV) using SS vs. Li at 60 °C.

Battery assembly and testing: In full cells, screen-printed LFP + LLZO (SP1) is used as composite cathodes and Li metal foil as anodes of 12 mm diameter, with CSE as electrolytes. The cells were closed with 800 KC pressure by a crimper. Galvanostatic charge-discharge tests were performed Maccor 4000 test system. The cells were rested at 60 °C for about 10 h before cycling between 2.5 and 4.0 V *vs.* Li at different current rates followed by long cycling at 0.5 C. Mass loading of the cathodes was in the range of 2–3 mg/cm^2. All the cell assemblies under the Argon glove box atmosphere conditions.

Supporting Information

The supplementary document is provided separately.

1. EDX mapping for the screen-printed composite cathode LFP + LLZO (Figure S1)
2. SEM images of Screen-printed composite cathode SP2 (LFP + LiTFSi) (Figure S2)
3. SEM cross-sectional view of CSE1 (PEO + LiTFSI + LLZO) and CSE2 (PEO + LiTFSI + LLZTO). (Figure S3)
4. Arrhenius plot of CSE1 (PEO + LiTFSi + LLZO) and CSE2 (PEO + LiTFSi + LLZTO) and Transference number obtained from the Nyquist plots results between 1 MHz to 0,01 mHz. (Figure S4)
5. Long cycling performances of Screen-printed composite cathode SP1 (LFP + LLZO) with EIS data. (Figure S5)
6. An initial cycling performance, Rate capability, and impedance data of Screen-printed composite cathode SP2 (LFP + LiTFSi). (Figure S6)

Acknowledgements

This work was supported and funded by EU/EURF (PASS, A76178) and EU/Interreg Nord (SolBat, grant no. 20202885) projects. D.D.R thanks to Academy of Finland – Academy Project (CEMGLASS-243033041) for financial support. Thanks, Dr. Gayathiri Peta and Dr. Miri Greenstein for the electrochemical measurements and their fruitful discussion.

Conflict of Interests

The authors declare no conflict of interest.

Data Availability Statement

The data that support the findings of this study are available from the corresponding author upon reasonable request.

Keywords: $LiFePO_4$ · solid-state batteries · hybrid electrolyte · screen printing · lithium metal

[1] R. M. Dell, *Solid State Ionics* **2000**, *134*, 139–158.
[2] H. Cavers, P. Molaiyan, M. Abdollahifar, U. Lassi, A. Kwade, *Adv. Energy Mater.* **2022**, *12*, 2200147.
[3] J. G. Kim, B. Son, S. Mukherjee, N. Schuppert, A. Bates, O. Kwon, M. J. Choi, H. Y. Chung, S. Park, *J. Power Sources* **2015**, *282*, 299–322.
[4] K. Takada, *Acta Mater.* **2013**, *61*, 759–770.
[5] J. T. Frith, M. J. Lacey, U. Ulissi, *Nat. Commun.* **2023**, *14*, 420.
[6] P. Molaiyan, M. Abdollahifar, B. Boz, A. Beutl, M. Krammer, N. Zhang, A. Tron, M. Romio, M. Ricci, R. Adelung, A. Kwade, U. Lassi, A. Paolella, *Adv. Funct. Mater.* **2023**, *n/a*, 2311301.
[7] J. Bae, S. Oh, B. Lee, C. H. Lee, J. Chung, J. Kim, S. Jo, S. Seo, J. Lim, S. Chung, *Energy Storage Mater.* **2023**, *57*, 277–288.
[8] Y. Liu, R. Zhang, J. Wang, Y. Wang, *iScience* **2021**, *24*, 102332.
[9] R. Sliz, P. Molaiyan, T. Fabritius, U. Lassi, *Nano Express* **2022**, *3*, 021002.
[10] W. S. Scheld, S. Lobe, C. Dellen, M. Ihrig, G. Häuschen, L. C. Hoff, M. Finsterbusch, S. Uhlenbruck, O. Guillon, D. Fattakhova-Rohlfing, *J. Power Sources* **2022**, *545*, 231872.
[11] S. Pinilla, S. Ryan, L. McKeon, M. Lian, S. Vaesen, A. Roy, W. Schmitt, J. N. Coleman, V. Nicolosi, *Adv. Energy Mater.* **2023**, *13*, 2203747, DOI 10.1002/aenm.202203747.
[12] R. Sliz, J. Valikangas, H. Silva Santos, P. Vilmi, L. Rieppo, T. Hu, U. Lassi, T. Fabritius, *ACS Appl. Energ. Mater.* **2022**, *5*, 4047–4058.
[13] A. Jabbar Khan, A. Mateen, S. Khan, L. He, W. Wang, A. Numan, K.-Q. Peng, I. Ahmed Malik, I. Hussain, G. Zhao, *Batteries & Supercaps* **2023**, *6*, e202300190.
[14] J. Wu, L. Yuan, W. Zhang, Z. Li, X. Xie, Y. Huang, *Energy Environ. Sci.* **2021**, *14*, 12–36.
[15] A. Gören, J. Mendes, H. M. Rodrigues, R. E. Sousa, J. Oliveira, L. Hilliou, C. M. Costa, M. M. Silva, S. Lanceros-Méndez, *J. Power Sources* **2016**, *334*, 65–77.
[16] V. Wurster, C. Engel, H. Graebe, T. Ferber, W. Jaegermann, R. Hausbrand, *J. Electrochem. Soc.* **2019**, *166*, A5410–A5420.
[17] N. Nitta, F. Wu, J. T. Lee, G. Yushin, *Mater. Today* **2015**, *18*, 252–264.
[18] P. Molaiyan, S. E. Mailhiot, K. Voges, A. M. Kantola, T. Hu, P. Michalowski, A. Kwade, V.-V. Telkki, U. Lassi, *Mater. Des.* **2023**, *227*, 111690.
[19] Q. Yu, K. Jiang, C. Yu, X. Chen, C. Zhang, Y. Yao, B. Jiang, H. Long, *Chin. Chem. Lett.* **2021**, *32*, 2659–2678.
[20] Z. Chen, G. T. Kim, Z. Wang, D. Bresser, B. Qin, D. Geiger, U. Kaiser, X. Wang, Z. X. Shen, S. Passerini, *Nano Energy* **2019**, *64*, 103986.
[21] N. Meng, X. Zhu, F. Lian, *Particuology* **2022**, *60*, 14–36.
[22] S. Liu, W. Liu, D. Ba, Y. Zhao, Y. Ye, Y. Li, J. Liu, *Adv. Mater.* **2023**, *35*, 2110423.
[23] D. Campanella, W. Zhu, G. Girard, S. Savoie, S. Kaboli, Z. Feng, A. Guerfi, M. Romio, P. Molaiyan, D. Bélanger, A. Paolella, *ChemSusChem* **2023**, *n/a*, e202300399.
[24] G. Yang, Y. Song, Q. Wang, L. Zhang, L. Deng, *Mater. Des.* **2020**, *190*, 108563.
[25] S. Luo, X. Liu, L. Gao, N. Deng, X. Sun, Y. Li, Q. Zeng, H. Wang, B. Cheng, W. Kang, *Sustain. Energy Fuels* **2022**, *6*, 5019–5044.
[26] R. Sliz, I. S. Roy, P. Molaiyan, J. Välikängas, T. Jakkila, M. H. Christophliemk, T. Hu, H. H. Nguyen, E. Hannila, S. Illikainen, U. Lassi, T. Fabritius, *Batter. Supercaps* **2024**, *n/a*, e202300527.
[27] M. Clausnitzer, R. Mücke, F. Al-Jaljouli, S. Hein, M. Finsterbusch, T. Danner, D. Fattakhova-Rohlfing, O. Guillon, A. Latz, *Batter. Supercaps* **2023**, *n/a*, e202300167.
[28] M. Dirican, C. Yan, P. Zhu, X. Zhang, *Mater. Sci. Eng. R* **2019**, *136*, 27–46.
[29] T. Zhang, W. He, W. Zhang, T. Wang, P. Li, Z. Sun, X. Yu, *Chem. Sci.* **2020**, *11*, 8686–8707.
[30] J. Guo, J. Zheng, W. Zhang, Y. Lu, *Energy Fuels* **2021**, *35*, 11118–11140.
[31] S. Sharifi-Asl, D. D. Macdonald, in *Dev. Electrochem. Sci. Inspired by Martin Fleischmann*, Wiley, **2014**, pp. 349–365, https://doi.org/10.1002/9781118694404.ch19.
[32] X. Zhao, C. Wang, H. Liu, Y. Liang, L.-Z. Fan, *Batteries & Supercaps* **2023**, *6*, e202200502.
[33] Z. Zhang, Y. Huang, H. Gao, J. Huang, C. Li, P. Liu, *Ceram. Int.* **2020**, *46*, 11397–11405.
[34] K. Pożyczka, M. Marzantowicz, J. R. Dygas, F. Krok, *Electrochim. Acta* **2017**, *227*, 127–135.
[35] O. Breuer, G. Peta, Y. Elias, H. Alon-Yehezkel, Y.-T. Weng, M. Fayena-Greenstein, N.-L. Wu, M. D. Levi, D. Aurbach, *J. Electrochem. Soc.* **2023**, *170*, 90509.
[36] S. Bublil, G. Peta, M. Fayena-Greenstein, H. Alon-Yehezkel, O. Raskin, Y. Elias, D. Aurbach, *J. Electrochem. Soc.* **2022**, *169*, 110523.
[37] P. Ravn Sørensen, T. Jacobsen, *Electrochim. Acta* **1982**, *27*, 1671–1675.

Manuscript received: February 19, 2024
Version of record online: ■■, ■■

RESEARCH ARTICLE

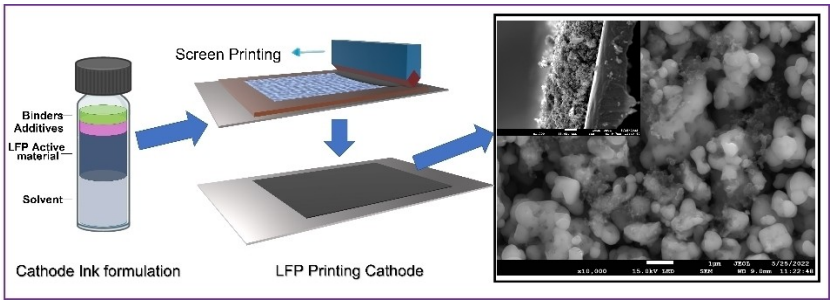

P. Molaiyan, J. Valikangas, R. Sliz, D. D. Ramteke, T. Hu, A. Paolella, T. Fabritius, U. Lassi**

1 – 8

Screen-Printed Composite $LiFePO_4$-LLZO Cathodes Towards Solid-State Li-ion Batteries

A screen-printing approach to prepare cathode composite based on LFP + LLZO is systematically designed and applied for SSB applications. With this approach, the screen-printed cathode paired with Li metal and composite solid electrolytes for SSB demonstrated better electrochemical performances and opened a gateway for new manufacturing techniques for future battery technology.